Classical and differential hardness – aspects of quantifying the deformation response in indentation experiments

Bodo Wolf

Classical and differential hardness Â aspects of quantifying the deformation response in indentation experiments

Journal:	*Philosophical Magazine & Philosophical Magazine Letters*
Manuscript ID:	TPHM-05-Nov-0498.R1
Journal Selection:	Philosophical Magazine
Date Submitted by the Author:	20-Jan-2006
Complete List of Authors:	Wolf, Bodo; Fachhochschule Lausitz, IEM
Keywords:	nanoindentation, contact mechanics, elasticity
Keywords (user supplied):	indentation modulus, indentation size effect, differential hardness

Classical and differential hardness – aspects of quantifying the deformation response in indentation experiments

BODO WOLF

Fachhochschule Lausitz , Fachbereich IEM, Großenhainer Straße 57, D-01968 Senftenberg, Germany

In depth sensing nanoindentation the load – depth-curve $F(h)$ is acquired from which a single value for the hardness H and a second one for the indentation modulus E_{ind} are inferred. This is a very poor output since $F(h)$ is a source of much more information. The paper describes a technique to extract the hardness $H(h)$ as a continuous depth dependent function from the load-depth-curve. This was accomplished by assigning each depth h a corresponding contact depth $h_C = h_C(h)$ that can be calculated using an iteration algorithm. The hardness is then simply $H(h) = F(h)/A_C(h_C(h))$. For very simple area functions A_C an analytical solution $h_C(h; F)$ can even be found. Furthermore, the differential hardness H_d is introduced as an additional hardness quantity which is obtained when dividing the load increment ΔF by the resulting increase of contact area ΔA_C It turns out, that H and H_d are identical quantities for a material of constant hardness only. When the hardness is depth and therefore size dependent, H_d differs from H in a definite way that depends on the hardness evolution with depth, i.e. on the indentation size effect of the material under investigation. The differential hardness proves particularly useful for inhomogeneous samples and situations where the hardness is time – dependent.

Keywords: Instrumented nanoindentation; Hardness; Elastic properties; Indentation modulus, Differential hardness, Indentation size effect

1. Introduction

The "classical" hardness measurement is a two-step process where first an impression is made, and after unloading the contact area is visualised using a suitable microscopy technique (light microscopy as well as electron microscopy or atomic force microscopy AFM) [1-3]. Its particular advantage is the easy separation of elastic and inelastic ("plastic") deformation. However, each experiment delivers one hardness quantity only, and elastic properties can only be derived in indirect manners (one possibility is the calculation of the elastic modulus from the shallowing of the impression grove [4]. The elastic redeformation in the centre of the impression is larger than at the brim, resulting in differences between the shapes of residual impression and impression body, respectively, from which the modulus may be inferred). In order to study the depth and size dependence of the hardness, impressions at different loads must be performed. The lateral sample inhomogeneity proves therefore an additional source of error for such investigations. Making the loads increasingly smaller complicates the localisation of the resulting impressions, and the relative error of the contact area measurement grows. These problems are mastered using the depth sensing indentation technique where load F and penetration depth h

are continuously sampled [5]. This allows for a tracking of the complete penetration process.

Some of the new generation nanoindentation machines are equipped with continuous stiffness measurement (CSM) facilities [6]. In this case a small force oscillation is superimposed onto the force ramping, and the depth response to this force modulation is recorded during penetration. This permits to continuously record load, depth and contact stiffness. For samples of constant elastic modulus the contact stiffness is easily related to the contact area (see equation 5), hence load F, depth h, contact area A_C and therefore hardness $H = F/A_C$ are derived as continuous depth functions. However, this is by far not implemented at all indentation equipment, and traditional indentation data analysis, based on the Oliver-Pharr-method [7, 8], delivers one single hardness value H and one value of the indentation modulus E_{ind} per indentation cycle only. The Oliver-Pharr-technique uses the unloading curve as predominant source of information, whereas the loading curve is not taken advantage of in this analysis approach. When having in mind, that the loading curve contains a lot of hidden information on the deformation response of the indented sample during the entire indentation process, a single value for both E_{ind} and H proves a very poor output. A much better output is accomplished in multicycling indentation tests [9]. Such a test consists of a series of i cycles of loading - partial unloading with stepwise increase of the maximum applied load. The partial unloading to a certain percentage of the applied load (typically10%...20%) is necessary, since the Oliver-Pharr-technique uses the initial elastic unloading stiffness S for the determination of the contact area A_C. Each cycle (cycle index i) delivers a set of data (F_i, h_i, h_{Ci}, A_{Ci}, S_i), from which the hardness (mean contact pressure)

$$H_i = F_i/A_{Ci} \tag{1}$$

and the indentation modulus

$$E_{ind,i} = \frac{S_i}{2\sqrt{A_{C_i}/\pi}} \tag{2}$$

are deduced (F_i: maximum cycle load, h_i: total penetration for the load F_i, h_{Ci}: contact depth for the load F_i, A_{Ci}: contact area, S_i: stiffness dF/dh at the beginning of unloading) . Though being a very efficient tool to obtain an overview on the evolution of hardness and indentation modulus with depth, there are good reasons why the multicycling is not applicable in every case:

i) The multicycling test lasts comparatively long, up to some minutes – depending on the number of cycles. Consequently, drift avoidance and precise drift correction are important issues. In case of instable thermal laboratory conditions the data, inferred from long lasting multicycling tests, are not reliable.

ii) A second point concerns the fact, that multicycling delivers discrete data only. There are many cases, where mechanical properties are required as continuous functions of the depth. A load-depth curve with discontinuities (pop-in events [10,11]) is a typical example. One wants to know the pressure at which initial yielding is initiated; and the pressure release due to the depth excursion is of interest, too. Since both load and depth excursion amplitude of a strain burst are subject to random scattering one cannot know in advance where one would have to unload to determine the pressures of interest by the multicycling technique.

iii) Point three hints at the fact that there are samples that do not stand repeated loading / unloading, since this can induce cracks or may result in indentation fatigue.
iv) Finally, indentation creep may result in strong deviations between mechanical properties, derived from a single cycle, and from multicycling experiments, respectively. Between creep speed dh/dt and applied stress σ a power law

$$\mathrm{d}h/\mathrm{d}t \sim \sigma^n \qquad (3)$$

is mostly found. Especially for hard materials (refractory metals, ceramics, glass) the stress exponent n is often very high, $n > 10$. This implies that a small load reduction drastically reduces the indentation creep. Hence the creep during unloading and reloading is negligible, apart from the direct neighbourhood of the maximum load of the indentation cycle, where the large stress results in a measurable indentation creep.
The situation is very different for a small stress exponent n in the range of 1 as found with plastics, e.g.. In this case creep persists during entire partial unloading and reloading; unloading and reloading curves do not coincide. Consequently, materials that exhibit a strong creep and a small stress exponent of the creep velocity are not suitable for multicycling indentation tests. In figure 1 the impact of indentation creep on load-depth curve $F(h)$ is schematically drawn for two materials with the same creep speed at maximum load of the cycle, but with different values of stress exponent n.

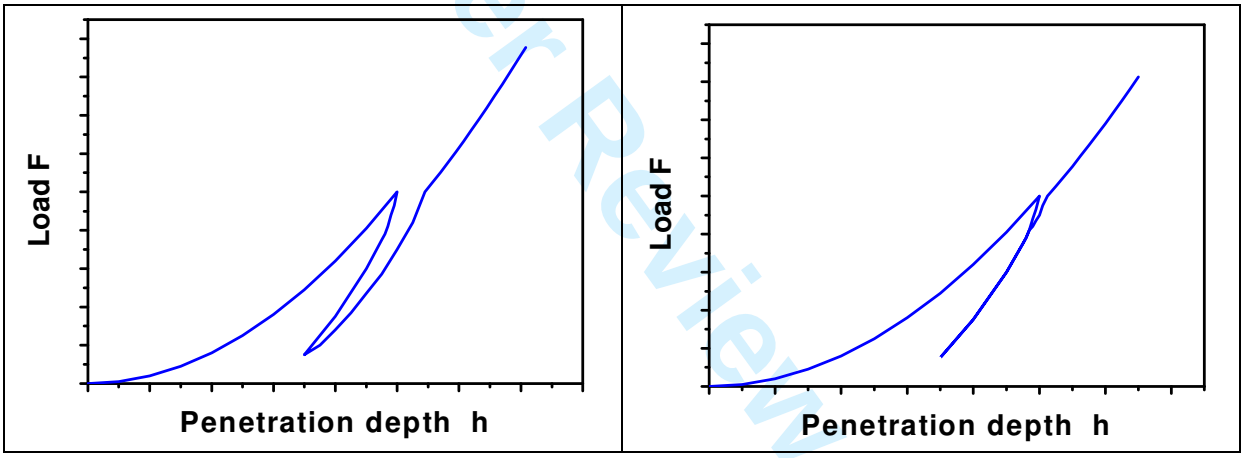

Figure 1
Principal sketch of the unloading-reloading-behaviour for materials with a small stress exponent n of creep (left graph) and a large stress exponent (right graph). For large values of n significant creep occurs in the vicinity of the maximum load only; for small n creep persists during entire unloading and reloading.

Summarizing we can state that the deduction of $H(h)$ from a single indentation cycle has some important advantages over the inference of discrete values H_i (h_i) from multicycling testing. The basic idea of the determination of $H(h)$ is to calculate the unloading curve for every point of the loading curve instead of measuring it. This requires the knowledge of the indentation modulus $E_{ind}(h)$ as a function of indentation depth h. The calculation is particularly easy for a homogeneous sample with constant elastic properties. In case of an inhomogeneous sample one can gain profit from the fact that $E_{ind}(h)$ will be a slowly varying function even in case of vary strong gradients of the elastic modulus $E(h)$ as for a multilayer system. To prove this one can argue that the indentation modulus E_{ind} is obtained from an elastically deformed volume the dimensions of which are large if compared to the indenter penetration depth.

Consequently, E_{ind} can only vary in a limited way, and it cannot exhibit discontinuities. It is therefore possible to measure $E_{ind,i}$ (h_i) for a small number of different depths h_i using either a multicycling test or some single tests at different loads, and to fit the discrete values $E_{ind,i}$ to a continuous function $E_{ind}(h)$ that represents the real depth evolution of E_{ind} with sufficient precision.

2. Calculation of the depth dependent hardness $H(h)$

The key point of the hardness calculation is to assign every total depth h a corresponding contact depth h_C. According to the Oliver-Pharr-algorithm [7, 8] this fundamental entity is given by

$$h_C = h - \varepsilon F/S \tag{4}$$

with ε being an indenter geometry-dependent constant, which does – and this is a real fortune – not much deviate from a mean value of 0.75 that is used in the following. The contact stiffness S writes

$$S = (dF/dh) = 2\, E_{ind} \sqrt{A_C/\pi} \tag{5}$$

We thus obtain

$$h_C = h - \frac{\varepsilon F}{2 E_r \sqrt{A_C / \pi}} \tag{6}$$

In this equation h_C occurs twice: in explicit form on the left side; implicitly it is contained in the contact area which is a function of h_C : $A_C = A_C(h_C)$. Equation 6 is suitable for iterative determination of h_C, which is necessary when A_C is a complicated mathematical function. This is normally the case when fitting the experimentally determined contact areas of a calibration procedure to a function

$$A_C(h_C) = C_2 h_C^{\,2} + C_1 h_C^{\,1} + C_{1/2} h_C^{\,1/2} + C_{1/4} h_C^{\,1/4} + C_{1/8} h_C^{\,1/8} + \ldots \tag{7}$$

as suggested by Oliver and Pharr [7].

Figure 2 shows the load-depth curves of both a single indent and a multi-indent into single-crystalline CdS (0001) using a comparatively blunt cube corner indenter. The maximum load is 3.9mN. For ease of recognition the single indent was shifted by 0.3mN. It is obvious that the loading curves of single indent and multi-indent are almost parallel, i. e. extended loading-unloading procedures do not strongly influence the sample hardness. In an indentation creep test the behaviour of CdS was found to be similar to that one which is schematically drawn in the right part of fig. 1. We can therefore expect that hardness values inferred from the multi-indent are approximately equivalent to those calculated from the $F(h)$-curve. This is demonstrated in fig. 3. It exhibits the hardness curves $H(h)$ of three successive iteration cycles which converge very rapidly. The deviation between calculated and measured hardness is smaller than 4%.

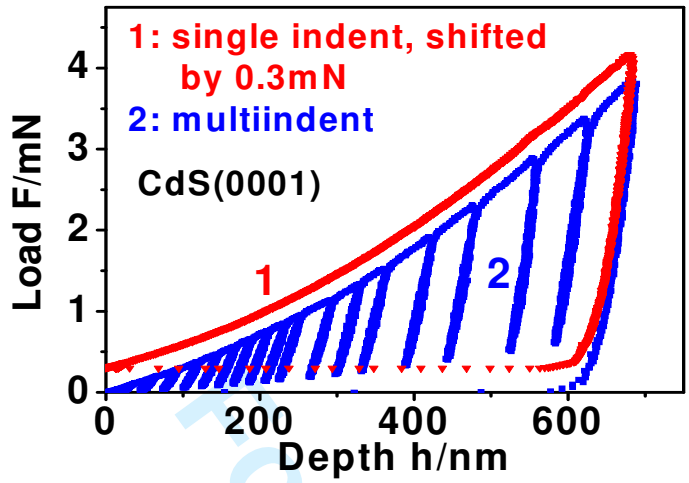

Fig. 2.
Load – depth-curves $F(h)$ of cube-corner indentations into CdS(0001)
Curve 1: Single indent
Curve 2: Multi-indent (18 cycles)
For better comparison curve 1 has been vertically shifted by 0.3mN.

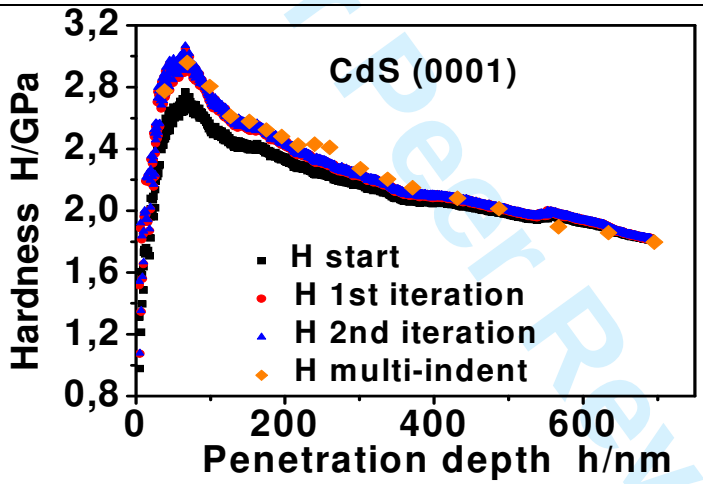

Fig. 3.
Hardness values derived from iterative analysis of a single indent (graph 1 in figure 2) compared to corresponding values inferred from a multicycling indentation (graph 2 in figure 2). The iteration procedure converges rapidly (iteration 2 is almost identical to iteration 1) and the obtained results are in good agreement to the multi-indentation data.

For very simple area functions $A_C(h_C)$ one can even find a closed analytical solution. For a cone or sphere A_C is simply given by

$$A_C = C_A\, h_C^2 \tag{8}$$

C_A is a constant that amounts to $C_A = 1.5\sqrt{3} = 2.6$ for a cube corner indenter, $C_A = 24.5$ for the Berkovich geometry, and $C_A = \pi \tan^2\alpha$ for a cone with α being half the angle at the tip of the cone [12]. We thus come to

$$h_C = h - \frac{\varepsilon F}{2E_{ind}\sqrt{A_C/\pi}} = \frac{h}{2} + \sqrt{\frac{h^2}{4} - \frac{\varepsilon F}{2E_{ind}\sqrt{C_A/\pi}}} \tag{9}$$

E_{ind} is considered as either constant or expressed as a function of total penetration depth h_t.

When a sphere of radius R is impressed down to a contact depth h_C, the corresponding contact radius r_C obeys the relation

$$r_C^2 = h_C(2R - h_C) \approx 2Rh_C \quad \text{for } R >> h_C \tag{10}$$

The contact area is

$$A_C = \pi\, r_C^2 = 2\pi R\, h_C \tag{11}$$

and it increases like a linear function with h_C. Combining equations (6) and (11) delivers

$$h_C^3 - 2h\,h_C^2 + h^2\,h_C - Q^2 = 0 \qquad Q = \frac{\varepsilon F}{2E_r\sqrt{2Rh_C}} \tag{12}$$

A solution of this third order equation can be found using the Cardanian solution formula, for practical purposes it is, however, more convenient to apply the iteration technique.

In the following let us consider a very interesting application of the h_C – calculation for a spherical indenter. In order to get deeper inside into the formation of dislocations as a result of a pop – in event one would like to know the irreversible plastic work connected to the depth excursion [10, 13]. This requires the determination of the area of the hysteresis loop formed by the $F(h)$-curves of elastic loading, depth excursion and elastic unloading immediately after the pop in (figure 4, left). This is experimentally difficult to accomplish since the load at which the strain burst is initiated (in the following called pop-load F_{pop}) and the amplitude of the depth excursion h_{pop} exhibit random scattering. As a consequence the expression

$$W_{pop} \approx F_{pop}\,h_{pop} \tag{13}$$

is simply used in literature [13], that is – however – too small. Owing to the increase of the contact area the unloading curve is stiffer than the loading curve.

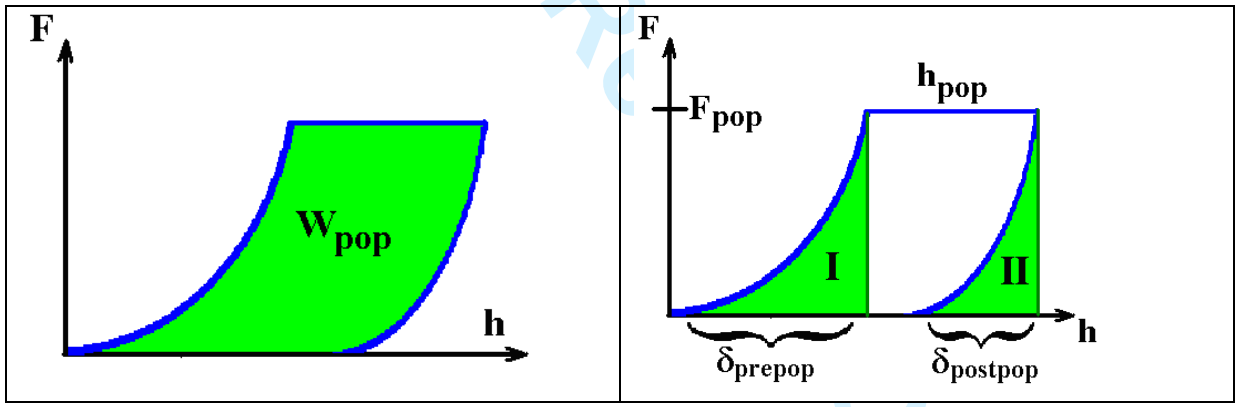

Figure 4
Schematical representation of the hysteresis loop of a strain burst event (left part). The areas beneath loading and unloading curve (regions I and II) are not equivalent, since the unloading is stiffer, resulting in $\delta_{prepop} < \delta_{postpop}$. Consequently, $W_{pop} > F_{pop}\,h_{pop}$ (right part).

The maximum elastic penetration at which the strain burst occurs is called δ_{prepop}; $\delta_{postpop}$ is the complete elastic recovery after the pop-in event. It can be concluded from fig. 4 that

$$W_{pop} = F_{pop}\,h_{pop} + W_I - W_{II}\ , \tag{14}$$

where W_I and W_{II} denote the areas beneath loading and unloading curve, respectively. Since the first pop-in mostly appears at tiny penetrations the part of the indenter tip in contact with the sample can be regarded as a sphere. For the elastic loading using a sphere HERTZ [14, 15] established a relation

$$F = K\,\delta^{3/2} \tag{15}$$

between load F and elastic penetration δ. The energy of elastic loading from $\delta = 0$ to $\delta = \delta_{max}$ is thus

$$W_{elast} = \int F \mathrm{d}\,\delta = = (2/5)\ F_{max}\ \delta_{max} \tag{16}$$

Introducing this into equation (14) gives

$$W_{pop} = F_{pop}\ h_{pop} + 0.4\ F_{pop}\ (\delta_{prepop} - \delta_{postpop}) \tag{17}$$

It is now necessary to express $\delta_{postpop}$ as a function of δ_{prepop} and h_{pop}. From equation (15) it follows, that the initial unloading stiffness $S = \mathrm{d}F/\mathrm{d}\delta$ can be written as

$$S_{prepop} = 1.5\ F_{pop}\ /\delta_{prepop} \qquad S_{postpop} = 1.5\ F_{pop}\ /\ \delta_{postpop} \tag{18}$$

Since E_{ind} before and after the pop-in event are equivalent the combination of (18) with (2) and (11) results in

$$\frac{\delta_{postpop}}{\delta_{prepop}} = \sqrt{\frac{A_{C,prepop}}{A_{C,postpop}}} = \sqrt{\frac{h_{C,prepop}}{h_{C,postpop}}} \tag{19}$$

According to HERTZ the elastic contact depth is half the total elastic penetration, i.e.

$$h_{C,prepop} = 0.5\delta_{prepop} \qquad h_{C,postpop} = h_t - 0.5\delta_{postpop} \tag{20}$$

$$\delta_{postpop} = \frac{\delta_{prepop}}{\sqrt{\frac{h_{C,postpop}}{h_{C,prepop}}}} = \frac{\delta_{prepop}}{\sqrt{\frac{h_t - 0.5\delta_{postpop}}{0.5\delta_{prepop}}}} \tag{21}$$

Equation (21) is suitable for iteration. For ease of demonstration let us consider the situation of $\delta_{postpop} = h_{pop} = a$. We thus have a total depth $h_t = 2a$ and $h_{C,prepop} = a/2$; starting the iteration with $\delta_{pospop,0} = a$ gives $h_{C,postpop,0} = 1.5a$. We obtain

$$\delta_{postpop,1} = a / \sqrt{1.5a / 0.5a} = a / \sqrt{3} = 0.58a$$

$$\delta_{postpop,\ 2} = a / \sqrt{(2a - 0.29\,a) / 0.5\,a} = 0.541\,a$$

$$\delta_{postpop,\ 3} = a / \sqrt{(2a - 0.27\ a) / 0.5\ a} = 0.538\ a$$

For the situation $h_{pop} = \delta_{prepop}$ a ratio $\delta_{postpop} / \delta_{prepop} = 0.54 \pm 0.005$ was found after 3 steps of iteration.

An interesting finding of the presented analysis is that the depth h_r of the remaining impression can be considerably larger than the depth excursion during the pop-in event. For the given example one obtains $h_r = 2a - \delta_{postpop} = 1.46a = 1.46h_{pop}$. In table 1 numerical values for the ratios $(\delta_{prepop}/\delta_{postpop})$ and (h_r/h_{pop}) and for the plastic energy W_{pop} are displayed as a function of the relative depth excursion $\alpha = h_{pop}/\delta_{prepop}$. It turns out that for tiny pop events, i.e. small values of α, the final depth is three times as large as the depth excursion, and the plastic energy approaches a value of $W_{pop} = 1.8\ F_{pop}\ h_{pop}$. This can be shown as follows:

$$\frac{\delta_{\mathrm{postpop}}}{\delta_{\mathrm{prepop}}} = \sqrt{\frac{A_{\mathrm{C,prepop}}}{A_{\mathrm{C,postpop}}}} = \sqrt{\frac{h_{\mathrm{C,prepop}}}{h_{\mathrm{C,postpop}}}} = \sqrt{\frac{\delta_{\mathrm{prepop}}/2}{\delta_{\mathrm{prepop}} + h_{\mathrm{pop}} - (\delta_{\mathrm{postpop}}/2)}} \tag{22}$$

$$\frac{\delta_{\mathrm{postpop}}}{\delta_{\mathrm{prepop}}} = \sqrt{\frac{1}{2 + 2(h_{\mathrm{pop}}/\delta_{\mathrm{prepop}}) - (\delta_{\mathrm{postpop}}/\delta_{\mathrm{prepop}})}} \tag{23}$$

We now introduce $\delta_{\mathrm{postpop}}/\delta_{\mathrm{prepop}} = 1 - 2\alpha$ and obtain with $h_{\mathrm{pop}}/\delta_{\mathrm{prepop}} = \alpha$

$$\frac{\delta_{\mathrm{postpop}}}{\delta_{\mathrm{prepop}}} = \sqrt{\frac{1}{1+4\alpha}} \approx \sqrt{1-4\alpha} \approx 1-2\alpha \tag{24}$$

i.e. we obtain a result which is consistent to the introduced prediction. Furthermore one gets

$$h_{\mathrm{r}} = \delta_{\mathrm{prepop}} + h_{\mathrm{pop}} - \delta_{\mathrm{postpop}} = h_{\mathrm{pop}} + 2\alpha\ \delta_{\mathrm{prepop}} \tag{25}$$

$$h_{\mathrm{r}}/h_{\mathrm{pop}} = 1 + 2\alpha\ (\delta_{\mathrm{prepop}}/h_{\mathrm{pop}}) = 1 + 2\alpha\ (1/\alpha) = 3 \tag{26}$$

$$\delta_{\mathrm{postpop}} - \delta_{\mathrm{prepop}} = 2\alpha\ \delta_{\mathrm{prepop}} = 2h_{\mathrm{pop}} \tag{27}$$

$$W_{\mathrm{pop}} = F_{\mathrm{pop}}\ h_{\mathrm{pop}} + 0.4\ F_{\mathrm{pop}}\ (\delta_{\mathrm{postpop}} - \delta_{\mathrm{prepop}}) = 1.8\ F_{\mathrm{pop}}\ h_{\mathrm{pop}} \tag{28}$$

relative depth excursion $\alpha = h_{\mathrm{pop}}/\delta_{\mathrm{prepop}}$	$\frac{\delta_{\mathrm{postpop}}}{\delta_{\mathrm{prepop}}}$	$\frac{h_{\mathrm{r}}}{h_{\mathrm{pop}}}$	Plastic energy W_{pop}
2	0.423	1.288	1.12 F_{pop} h_{pop}
1	0.537	1.463	1.19 F_{pop} h_{pop}
0.5	0.653	1.694	1.27 F_{pop} h_{pop}
0,2	0.788	2.06	1.42 F_{pop} h_{pop}
0.1	0.867	2.33	1.53 F_{pop} h_{pop}
0.01	0.981	2.90	1.77 F_{pop} h_{pop}
0.001	0.9980	3.00	1.80 F_{pop} h_{pop}
$\alpha << 1$	$1 - 2\alpha$	3.00	1.80 F_{pop} h_{pop}

Table 1
Characteristic quantities of a loading-unloading loop involving a depth excursion. The data were calculated as a function of the relative depth excursion amplitude $\alpha = h_{\mathrm{pop}}/\delta_{\mathrm{prepop}}$

The most interesting outcome of table 1 is that for small pop-in events the remaining depth oh the impression grove is three times as large as the depth excursion, and the plastic work is almost double the value of F_{pop} h_{pop}. This theoretical finding was confirmed by experiments. Figure 5 displays the load-depth curve $F(h)$ for a Berkovich nanoindent into single-crystalline GaAs(100). The maximum load was 100µN, and this was by chance only a bit larger than the pop-in force of approximately 90µN. The depth excursion amounts to h_{pop} = 2nm, whereas the remaining depth is 6nm, i.e. three times as large. The average spacing between loading and unloading curve is d = 0.5(2nm + 6nm) = 4nm, i.e. twice as large as h_{pop}. The content of the loading-unloading loop amounts to $A_{\mathrm{loop}} = W_{\mathrm{pop}} \approx F_{\mathrm{pop}}\ d \approx 2\ F_{\mathrm{pop}}\ h_{\mathrm{pop}}$ in good agreement to the theoretical value of $W_{\mathrm{pop}} = 1.8\ F_{\mathrm{pop}}\ h_{\mathrm{pop}}$.

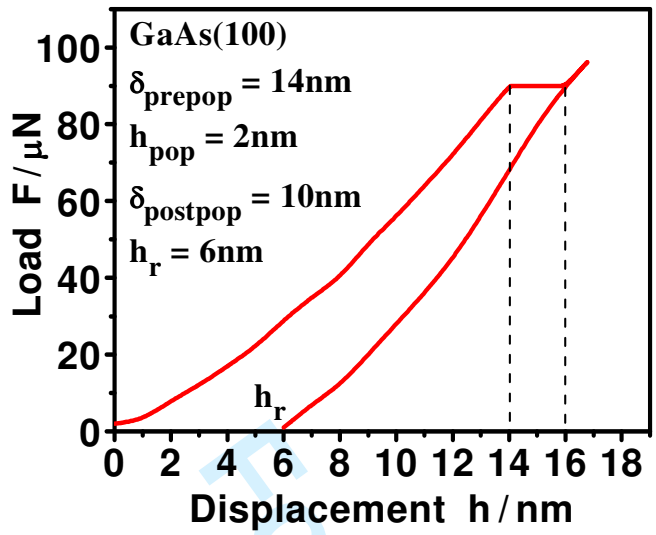

Fig. 5
Cube corner nanoindentation into GaAs (100). By chance the pop-in event occurs close to the termination of the loading segment which permits an experimental test of the predictions of Table 1.

3. The concept of differential hardness

The traditional nanohardness $H = F/A_C$ is the mean pressure inside the contact area of the indenter. If considering a multi-indentation test one can also divide the load increment ΔF from cycle to cycle by the corresponding increase of the contact area ΔA_C. This quantity is now introduced as "differential" hardness H_d:

$$H_d = \Delta F/\Delta A_C \qquad (29)$$

The multi-indent delivers discrete values of H_d. In figure 6A values of H and H_d derived from multi-indentation testing of Cu (100) are depicted. The differential hardness was found to be smaller than the traditional hardness. As will be shown below this difference is related to the indentation size effect of Cu, i.e. the general decrease of hardness with increasing penetration depth in the nanorange. When considering materials of constant hardness, the values of H and H_d are equivalent.

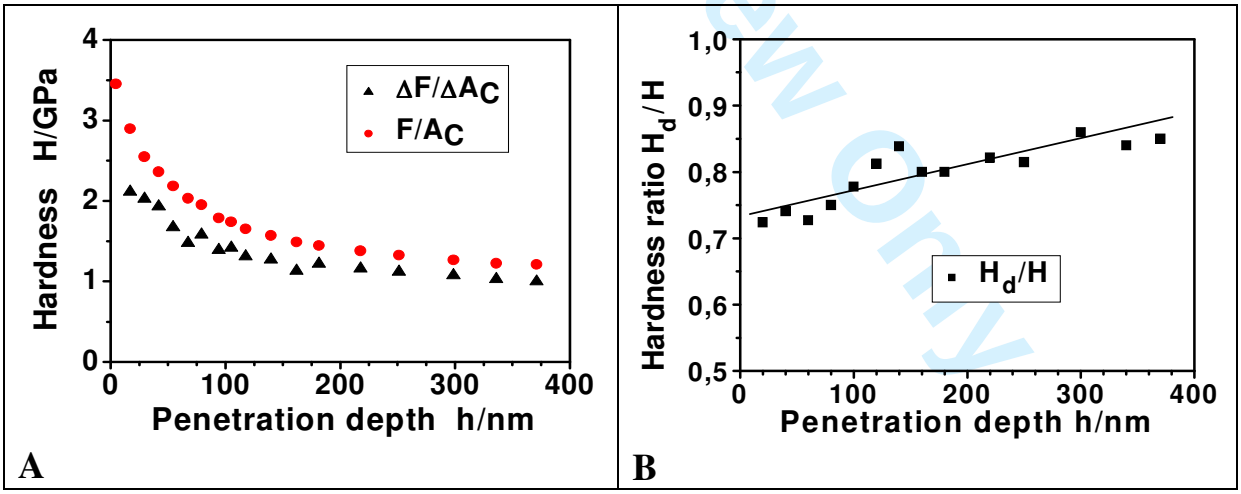

Figure 6
A) Traditional nanohardness data $H = F/A_C$ compared to corresponding values of the differential hardness $H_d = \Delta F/\Delta A_C$ as taken from multi-indentation testing of Cu (100).
B) Ratio H_d/H for the measurement of figure 6A exhibiting a typical value of $H_d/H \approx 0.75$ with the tendency of a slight increase from about 0.73 to 0.85 with increasing depth as indicated by the trend line.

The differential hardness can also be derived from a single indent:

$$H_d = dF/dA_C = (dF/dh)/(dA_C/dh) \quad (30)$$

To calculate H_d we need the differential quotient dF/dh which is simply the slope of the $F(h)$-curve. Additionally, dA_C/dh is required which is not directly accessible from the experiment. However, we know A_C as a function of contact depth h_C. Thus we can write

$$dA_C/dh = (dA_C/dh_C)*(dh_C/dh) \quad (31)$$

(dA_C/dh_C) is accessible from the indenter shape calibration. Furthermore, we can assume that (dh_C/dh) is a function that exhibits small variations with depth h only. Thus we can write

$$dh_C/dh \approx h_C/h \quad (32)$$

where h_C and h are the values of contact depth and total depth taken from the final unloading procedure. This results in

$$H_d = (dF/dh)/[(dA_C/dh_C)*(dh_C/dh)] \approx (h/h_C)*(dF/dh)/(dA_C/dh_C) \quad (33)$$

4. Relation between traditional hardness H and differential hardness H_d

We start with the definition of classical hardness $H = F/A_C$ and perform some simple transformations:

$$HA_C = F \quad (34)$$

$$HA_C = \int dF = \int \frac{dF}{dA_C} * \frac{dA_C}{dh} * dh = \int H_d * \frac{dA_C}{dh} * dh \quad (35)$$

After the operations (d/dh) and division by (dA_C/dh) one obtains

$$H_d = H + \frac{dH}{dh} * \frac{A_C}{(dA_C/dh_C)(dh_C/dh)} \quad (36)$$

For an ideal pointed indenter (pyramid / cone) the area function is $A_C = C_A h_C^2$, resulting in $dA_C/dh_C = 2C_A h_C$. This in combination with $dh_C/dh \approx h_C/h$ delivers

$$H_d = H + \frac{1}{2}\frac{dH}{dh} * h \quad (37)$$

We see that for missing indentation size effect ($dH/dh = 0$) the relation $H_d = H$ is obtained. The normal indentation size effect ($dH/dh < 0$) results in a differential hardness which is smaller than H. Such a situation can be found with tiny indentations into single-crystalline metals where the hardness can be described following the model of geometrical necessary dislocations [16, 17], as in the case of copper, e.g. . The model of geometrical necessary dislocations predicts a depth dependence of H according to

$$H = H_0\sqrt{\frac{h^*}{h}} \quad (38)$$

with H_0 and h^* being scaling parameters that depend on the defect structure of the metal. This delivers

$$H_d = H + \frac{1}{2}\frac{dH}{dh}h = (3/4)\,H \qquad (39)$$

A closer look to figure 6B reveals that H_d/H indeed scatters around 0.75 with a slight tendency to increase with deeper penetration which is further discussed in the following section.

5. Application of differential hardness and conclusions

The differential hardness as a differential entity is of course more inclined to scatter and it is more sensitive to measurement errors than traditional hardness or integral techniques as the derivation of an energetic hardness from the plastic work during indentation, e.g. Since H_d and H have the same value for homogeneous materials and self-similar indents the application of the differential hardness concept to such situations does indeed not provide new information. The situation is completely different with inhomogeneous samples, as layer systems, e. g. It should be noticed here that even a small pyramid indent into a single crystal will not obey the criteria of self-similarity though the indentation body is self similar. The deformation can be roughly separated into two stages:

Stage I: Small penetrations where the indent size is not much larger than the mean distance between hardness determining crystal defects. Here the hardness is governed by dislocations and other defects created by the indenter itself. The density of these defects depends on indent size, consequently the situation is not self-similar, and the hardness varies.

Stage II: Large penetrations, where the hardness is determined by intrinsically existing lattice defects. Provided the defect distribution is homogeneous the indent is self-similar, and the hardness is constant. Then $dH/dh = 0$, and $H_d/H = 1$ is found.

The slow increase of H_d/H in figure 6B indicates the transition from stage I to stage II, and from the trend may be concluded that stage II will dominate after about 2µm of penetration.

In case of "really" inhomogeneous specimens as layered materials one wants to know the single layer properties, but even the depth dependent hardness is no direct measure of the material property at the corresponding depth owing to the averaging over a larger deformed volume. To extract the real material property in a certain depth a deconvolution must be made. To do this one has to know to what extent material properties at a depth $h + \Delta h$ contribute to the measured data at depth h. It is reasonable to assume, that these contributions to H and H_d are different. Hence H_d is an additional source of information to make the deconvolution procedure more straightforward.

Another field of application are processes that occur during the indentation test itself and modify the sample hardness. As an example the photoplastic effect (PPE) shall be considered here. Some materials – II-VI-semiconductors in particular – change their hardness reversibly when illuminated by light the photon energy of which is sufficient to initiate the internal photo-electric effect. This finding is explained by electrical charging of dislocations [18]; indentation studies of the PPE in ZnSe have been reported in [19]. Figure 7 displays two load-depth-curves $F(h)$ of nanoindentations into the II-VI-semiconductor ZnSe. The sudden change of the slope of curve 1 was induced by turning a laser on which resulted in a positive photoplastic effect (reverse material hardening). Curve 2 belongs to an indentation completely performed in darkness. The difference of the final penetrations between curves 1 and 2 is about 30nm or 5% of the total depth, resulting in about 10% hardness change, only (for pyramid indenters the

relative hardness change is about twice the relative depth variation). This apparently small effect originates from the fact that the illumination was turned on close to the end of the indentation process when most of the deformation was already done. On the other hand the slope changes from $(dF/dh)_{dark}$ = 47µN/nm to $(dF/dh)_{light}$ = 83µN/nm. This means, that the differential hardness – representing the instantaneous deformation resistance – has almost doubled in contrast to the "traditional" hardness, which increased by 10%. When modulating the light intensity the penetration curve oscillates, and the differential hardness proves a suitable tool to track the corresponding hardness evolution. Summarizing we can say, that the differential hardness may be particularly advantageous when time dependent processes that affect the hardness occur during the indentation process itself.

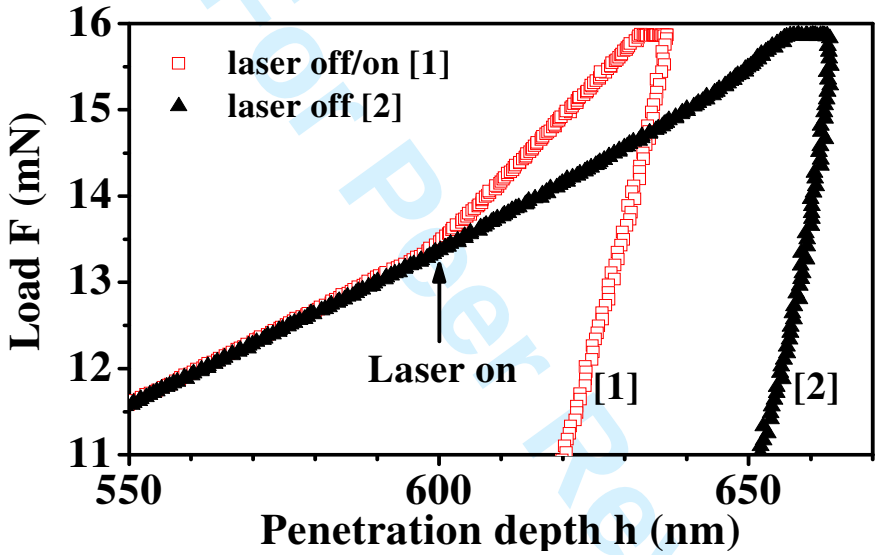

Figure 7.
Response of the load-depth-curve of a Berkovich nanoindention into ZnSe (111) to sudden illumination by laser light (λ = 543nm, intensity I = 120mW/cm^2). Curve 1: starting the indent in darkness the laser was turned on at a total depth h = 600nm. Curve 2: indentation in permanent darkness.

Acknowledgments
The experimental results used in this paper were obtained during stays of the author at Technische Universität Dresden, Technische Fachhochschule Wildau (Laboratory of Surface Physics, Prof. Asta Richter) and Universität des Saarlandes, Saarbrücken. The author would like to express his gratitude to the staff of these institutions for very fruitful cooperation.

References

[1] D. Tabor, *The hardness of metals* (Clarendon Press, Oxford, 1951).

[2] B.W. Mott, *Micro-indentation hardness testing* (Butterworths, London, 1956).

[3] J.L. Hay, G.M. Pharr, in *ASM Metals Handbook* (ASM International, Materials Park, Ohio, 2000).

[4] B. Wolf and P. Paufler, phys. stat. sol. (a) **172** 341 (1999).

[5] B. Bhushan, in *Springer Handbook of Nanotechnology*, edited by B. Bhushan (Springer, Berlin, New York, 2004) Chapter 22, pp. 685 - 714.

[6] Nano Instruments Website (2006 MTS Systems Corporation) available online at: http://www.mtsnano.com/products/csm/

[7] W.C. Oliver and G.M. Pharr, J. Mater. Res. **7** 1564 (1992).

[8] W.C. Oliver and G.M. Pharr, J. Mater. Res. **19** 3 (2004).

[9] B. Wolf, A. Richter and M. Günther, Z. Metallkd. **94** 807 (2003).

[10] D.F. Bahr, D.E. Wilson and D.A. Crowson, J. Mater. Res. **14** 2269 (1999).

[11] E.B. Tadmor, R. Miller, R. Phillips and M. Ortiz, J. Mater. Res. **14** 2233 (1999).

[12] B. Wolf, Cryst. Res. Technol. **35** 377 (2000).

[13] A. Zeckzer, Anisotropie der Versetzungsnukleation in GaAs bei Nanoindentierung, PhD thesis, Martin-Luther-Universität Halle-Wittenberg (2002).

[14] H. Hertz, J. reine und angewandte Mathematik **92** 156 (1882).

[15] K.L. Johnson, *Contact mechanics* (Cambridge University Press, Cambridge, 1985).

[16] M.F. Ashby, Phil. Mag. **21** 399 (1970).

[17] S. Sun, B.L. Adams and W.E. King, Phil. Mag. **A80** 9 (2000).

[18] Yu.A.Osiyan, V.F. Petrenko, A.V. Zaretskij and R.W. Whitworth, Adv. Phys. **35** 115 (1986).

[19] B. Wolf, A. Belger, D.C. Meyer and P. Paufler, phys. stat. sol. (a) **187** 415 (2001) and Phil. Mag. A **82** 1865 (2002).

Figure Captions / Table Legends

Figure 1
Principal sketch of the unloading-reloading-behaviour for materials with a small stress exponent n of creep (left graph) and a large stress exponent (right graph). For large values of n significant creep occurs in the vicinity of the maximum load only; for small n creep persists during entire unloading and reloading.

Fig. 2.
Load – depth-curves $F(h)$ of cube-corner indentations into CdS(0001)
Curve 1: Single indent
Curve 2: Multi-indent (18 cycles)
For better comparison curve 1 was vertically shifted by 0.3mN.

Fig. 3.
Hardness values derived from iterative analysis of a single indent (graph 1 in figure 2) compared to corresponding values inferred from a multicycling indentation (graph 2 in figure 2). The iteration procedure converges rapidly (iteration 2 is almost identical to iteration 1) and the obtained results are in good agreement to the multi-indentation data.

Figure 4
Schematical representation of the hysteresis loop of a strain burst event (left part). The areas beneath loading and unloading curves (regions I and II) are not equivalent, since the unloading is stiffer, resulting in $\delta_{prepop} < \delta_{postpop}$. Consequently, $W_{pop} > F_{pop}\, h_{pop}$ (right part).

Fig. 5
Cube corner nanoindentation into GaAs (100). By chance the pop-in event occurs close to the termination of the loading segment which permits an experimental test of the predictions of table 1.

Figure 6
A) Traditional nanohardness data $H = F/A_C$ compared to corresponding values of the differential hardness $H_d = \Delta F/\Delta A_C$ as taken from multi-indentation testing of Cu (100).
B) Ratio H_d/H for the measurement of figure 6A exhibiting a typical value of $H_d/H \approx 0.75$ with the tendency of a slight increase from about 0.73 to 0.85 with increasing depth as indicated by the trend line.

Figure 7.
Response of the load-depth-curve of a Berkovich nanoindention into ZnSe (111) to sudden illumination by laser light (λ = 543nm, intensity I = 120mW/cm^2). Curve 1: starting the indent in darkness the laser was turned on at a total depth h = 600nm. Curve 2: indentation in permanent darkness.

Table legends

Table 1
Characteristic quantities of a loading-unloading loop involving a depth excursion. The data were calculated as a function of the relative depth excursion amplitude $\alpha = h_{pop}/\delta_{prepop}$

Classical and differential hardness – aspects of quantifying the deformation response in indentation experiments

BODO WOLF

Fachhochschule Lausitz , Fachbereich IEM, Großenhainer Straße 57, D-01968 Senftenberg, Germany

In depth sensing nanoindentation the load – depth-curve $F(h)$ is acquired from which a single value for the hardness H and a second one for the indentation modulus E_{ind} are inferred. This is a very poor output since $F(h)$ is a source of much more information. The paper describes a technique to extract the hardness $H(h)$ as a continuous depth dependent function from the load-depth-curve. This was accomplished by assigning each depth h a corresponding contact depth $h_C = h_C(h)$ that can be calculated using an iteration algorithm. The hardness is then simply $H(h) = F(h)/A_C(h_C(h))$. For very simple area functions A_C an analytical solution $h_C(h; F)$ can even be found. Furthermore, the differential hardness H_d is introduced as an additional hardness quantity which is obtained when dividing the load increment ΔF by the resulting increase of contact area ΔA_C It turns out, that H and H_d are identical quantities for a material of constant hardness only. When the hardness is depth and therefore size dependent, H_d differs from H in a definite way that depends on the hardness evolution with depth, i.e. on the indentation size effect of the material under investigation. The differential hardness proves particularly useful for inhomogeneous samples and situations where the hardness is time – dependent.

Keywords: Instrumented nanoindentation; Hardness; Elastic properties; Indentation modulus, Differential hardness, Indentation size effect

1. Introduction

The "classical" hardness measurement is a two-step process where first an impression is made, and after unloading the contact area is visualised using a suitable microscopy technique (light microscopy as well as electron microscopy or atomic force microscopy AFM) [1-3]. Its particular advantage is the easy separation of elastic and inelastic ("plastic") deformation. However, each experiment delivers one hardness quantity only, and elastic properties can only be derived in indirect manners (one possibility is the calculation of the elastic modulus from the shallowing of the impression grove [4]. The elastic redeformation in the centre of the impression is larger than at the brim, resulting in differences between the shapes of residual impression and impression body, respectively, from which the modulus may be inferred). In order to study the depth and size dependence of the hardness, impressions at different loads must be performed. The lateral sample inhomogeneity proves therefore an additional source of error for such investigations. Making the loads increasingly smaller complicates the localisation of the resulting impressions, and the relative error of the contact area measurement grows. These problems are mastered using the depth sensing indentation technique where load F and penetration depth h

are continuously sampled [5]. This allows for a tracking of the complete penetration process.

Some of the new generation nanoindentation machines are equipped with continuous stiffness measurement (CSM) facilities [6]. In this case a small force oscillation is superimposed onto the force ramping, and the depth response to this force modulation is recorded during penetration. This permits to continuously record load, depth and contact stiffness. For samples of constant elastic modulus the contact stiffness is easily related to the contact area (see equation 5), hence load F, depth h, contact area A_C and therefore hardness $H = F/A_C$ are derived as continuous depth functions. However, this is by far not implemented at all indentation equipment, and traditional indentation data analysis, based on the Oliver-Pharr-method [7, 8], delivers one single hardness value H and one value of the indentation modulus E_{ind} per indentation cycle only. The Oliver-Pharr-technique uses the unloading curve as predominant source of information, whereas the loading curve is not taken advantage of in this analysis approach. When having in mind, that the loading curve contains a lot of hidden information on the deformation response of the indented sample during the entire indentation process, a single value for both E_{ind} and H proves a very poor output. A much better output is accomplished in multicycling indentation tests [9]. Such a test consists of a series of i cycles of loading - partial unloading with stepwise increase of the maximum applied load. The partial unloading to a certain percentage of the applied load (typically10%...20%) is necessary, since the Oliver-Pharr-technique uses the initial elastic unloading stiffness S for the determination of the contact area A_C. Each cycle (cycle index i) delivers a set of data (F_i, h_i, h_{Ci}, A_{Ci}, S_i), from which the hardness (mean contact pressure)

$$H_i = F_i/A_{Ci} \tag{1}$$

and the indentation modulus

$$E_{ind,i} = \frac{S_i}{2\sqrt{A_{c_i}/\pi}} \tag{2}$$

are deduced (F_i: maximum cycle load, h_i: total penetration for the load F_i, h_{Ci}: contact depth for the load F_i, A_{Ci}: contact area, S_i: stiffness dF/dh at the beginning of unloading) . Though being a very efficient tool to obtain an overview on the evolution of hardness and indentation modulus with depth, there are good reasons why the multicycling is not applicable in every case:

i) The multicycling test lasts comparatively long, up to some minutes – depending on the number of cycles. Consequently, drift avoidance and precise drift correction are important issues. In case of instable thermal laboratory conditions the data, inferred from long lasting multicycling tests, are not reliable.

ii) A second point concerns the fact, that multicycling delivers discrete data only. There are many cases, where mechanical properties are required as continuous functions of the depth. A load-depth curve with discontinuities (pop-in events [10,11]) is a typical example. One wants to know the pressure at which initial yielding is initiated; and the pressure release due to the depth excursion is of interest, too. Since both load and depth excursion amplitude of a strain burst are subject to random scattering one cannot know in advance where one would have to unload to determine the pressures of interest by the multicycling technique.

iii) Point three hints at the fact that there are samples that do not stand repeated loading / unloading, since this can induce cracks or may result in indentation fatigue.
iv) Finally, indentation creep may result in strong deviations between mechanical properties, derived from a single cycle, and from multicycling experiments, respectively. Between creep speed dh/dt and applied stress σ a power law

$$dh/dt \sim \sigma^n \quad (3)$$

is mostly found. Especially for hard materials (refractory metals, ceramics, glass) the stress exponent n is often very high, $n > 10$. This implies that a small load reduction drastically reduces the indentation creep. Hence the creep during unloading and reloading is negligible, apart from the direct neighbourhood of the maximum load of the indentation cycle, where the large stress results in a measurable indentation creep.
The situation is very different for a small stress exponent n in the range of 1 as found with plastics, e.g.. In this case creep persists during entire partial unloading and reloading; unloading and reloading curves do not coincide. Consequently, materials that exhibit a strong creep and a small stress exponent of the creep velocity are not suitable for multicycling indentation tests. In figure 1 the impact of indentation creep on load-depth curve $F(h)$ is schematically drawn for two materials with the same creep speed at maximum load of the cycle, but with different values of stress exponent n.

INSERT FIGURE 1 ABOUT HERE

Summarizing we can state that the deduction of $H(h)$ from a single indentation cycle has some important advantages over the inference of discrete values H_i (h_i) from multicycling testing. The basic idea of the determination of $H(h)$ is to calculate the unloading curve for every point of the loading curve instead of measuring it. This requires the knowledge of the indentation modulus $E_{ind}(h)$ as a function of indentation depth h. The calculation is particularly easy for a homogeneous sample with constant elastic properties. In case of an inhomogeneous sample one can gain profit from the fact that $E_{ind}(h)$ will be a slowly varying function even in case of vary strong gradients of the elastic modulus $E(h)$ as for a multilayer system. To prove this one can argue that the indentation modulus E_{ind} is obtained from an elastically deformed volume the dimensions of which are large if compared to the indenter penetration depth. Consequently, E_{ind} can only vary in a limited way, and it cannot exhibit discontinuities. It is therefore possible to measure $E_{ind,i}$ (h_i) for a small number of different depths h_i using either a multicycling test or some single tests at different loads, and to fit the discrete values $E_{ind,i}$ to a continuous function $E_{ind}(h)$ that represents the real depth evolution of E_{ind} with sufficient precision.

2. Calculation of the depth dependent hardness $H(h)$

The key point of the hardness calculation is to assign every total depth h a corresponding contact depth h_C. According to the Oliver-Pharr-algorithm [7, 8] this fundamental entity is given by

$$h_C = h - \varepsilon F/S \quad (4)$$

with ε being an indenter geometry-dependent constant, which does – and this is a real fortune – not much deviate from a mean value of 0.75 that is used in the following. The contact stiffness S writes

$$S = (\mathrm{d}F/\mathrm{d}h) = 2\, E_{\mathrm{ind}} \sqrt{A_C/\pi} \tag{5}$$

We thus obtain

$$h_C = h - \frac{\varepsilon F}{2 E_r \sqrt{A_C / \pi}} \tag{6}$$

In this equation h_C occurs twice: in explicit form on the left side; implicitly it is contained in the contact area which is a function of h_C : $A_C = A_C(h_C)$. Equation 6 is suitable for iterative determination of h_C, which is necessary when A_C is a complicated mathematical function. This is normally the case when fitting the experimentally determined contact areas of a calibration procedure to a function

$$A_C(h_C) = C_2 h_C^{\,2} + C_1 h_C^{\,1} + C_{1/2} h_C^{\,1/2} + C_{1/4} h_C^{\,1/4} + C_{1/8} h_C^{\,1/8} + \ldots \tag{7}$$

as suggested by Oliver and Pharr [7].

Figure 2 shows the load-depth curves of both a single indent and a multi-indent into single-crystalline CdS (0001) using a comparatively blunt cube corner indenter. The maximum load is 3.9mN. For ease of recognition the single indent was shifted by 0.3mN. It is obvious that the loading curves of single indent and multi-indent are almost parallel, i. e. extended loading-unloading procedures do not strongly influence the sample hardness. In an indentation creep test the behaviour of CdS was found to be similar to that one which is schematically drawn in the right part of fig. 1. We can therefore expect that hardness values inferred from the multi-indent are approximately equivalent to those calculated from the $F(h)$-curve. This is demonstrated in fig. 3. It exhibits the hardness curves $H(h)$ of three successive iteration cycles which converge very rapidly. The deviation between calculated and measured hardness is smaller than 4%.

INSERT FIGURES 2 AND 3 ABOUT HERE

For very simple area functions $A_C(h_C)$ one can even find a closed analytical solution. For a cone or sphere A_C is simply given by

$$A_C = C_A\, h_C^2 \tag{8}$$

C_A is a constant that amounts to $C_A = 1.5\sqrt{3} = 2.6$ for a cube corner indenter, $C_A = 24.5$ for the Berkovich geometry, and $C_A = \pi \tan^2\alpha$ for a cone with α being half the angle at the tip of the cone [12]. We thus come to

$$h_C = h - \frac{\varepsilon F}{2E_{ind}\sqrt{A_C/\pi}} = \frac{h}{2} + \sqrt{\frac{h^2}{4} - \frac{\varepsilon F}{2E_{ind}\sqrt{C_A/\pi}}} \tag{9}$$

E_{ind} is considered as either constant or expressed as a function of total penetration depth h_t.

When a sphere of radius R is impressed down to a contact depth h_C, the corresponding contact radius r_C obeys the relation

$$r_C^2 = h_C(2R - h_C) \approx 2Rh_C \quad \text{for } R >> h_C \tag{10}$$

The contact area is

$$A_C = \pi\, r_C^2 = 2\pi R\, h_C \tag{11}$$

and it increases like a linear function with h_C. Combining equations (6) and (11) delivers

$$h_C^3 - 2h\, h_C^2 + h^2\, h_C - Q^2 = 0 \qquad Q = \frac{\varepsilon F}{2E_r\sqrt{2Rh_C}} \tag{12}$$

A solution of this third order equation can be found using the Cardanian solution formula, for practical purposes it is, however, more convenient to apply the iteration technique.

In the following let us consider a very interesting application of the h_C – calculation for a spherical indenter. In order to get deeper inside into the formation of dislocations as a result of a pop – in event one would like to know the irreversible plastic work connected to the depth excursion [10, 13]. This requires the determination of the area of the hysteresis loop formed by the $F(h)$-curves of elastic loading, depth excursion and elastic unloading immediately after the pop in (figure 4, left). This is experimentally difficult to accomplish since the load at which the strain burst is initiated (in the following called pop-load F_{pop}) and the amplitude of the depth excursion h_{pop} exhibit random scattering. As a consequence the expression

$$W_{pop} \approx F_{pop}\, h_{pop} \tag{13}$$

is simply used in literature [13], that is – however – too small. Owing to the increase of the contact area the unloading curve is stiffer than the loading curve.

INSERT FIGURE 4 ABOUT HERE

The maximum elastic penetration at which the strain burst occurs is called δ_{prepop}; $\delta_{postpop}$ is the complete elastic recovery after the pop-in event. It can be concluded from fig. 4 that

$$W_{pop} = F_{pop}\, h_{pop} + W_I - W_{II} \ , \tag{14}$$

where W_I and W_{II} denote the areas beneath loading and unloading curve, respectively. Since the first pop-in mostly appears at tiny penetrations the part of the indenter tip in contact with the sample can be regarded as a sphere. For the elastic loading using a sphere HERTZ [14, 15] established a relation

$$F = K\, \delta^{3/2} \tag{15}$$

between load F and elastic penetration δ. The energy of elastic loading from $\delta = 0$ to $\delta = \delta_{max}$ is thus

$$W_{elast} = \int F \mathrm{d}\,\delta = = (2/5)\, F_{max}\, \delta_{max} \tag{16}$$

Introducing this into equation (14) gives

$$W_{pop} = F_{pop}\, h_{pop} + 0.4\, F_{pop}\, (\delta_{prepop} - \delta_{postpop}) \tag{17}$$

It is now necessary to express $\delta_{postpop}$ as a function of δ_{prepop} and h_{pop}. From equation (15) it follows, that the initial unloading stiffness $S = \mathrm{d}F/\mathrm{d}\delta$ can be written as

$$S_{prepop} = 1.5\, F_{pop}\, /\delta_{prepop} \qquad S_{postpop} = 1.5\, F_{pop}\, /\, \delta_{postpop} \tag{18}$$

Since E_{ind} before and after the pop-in event are equivalent the combination of (18) with (2) and (11) results in

$$\frac{\delta_{postpop}}{\delta_{prepop}} = \sqrt{\frac{A_{C,prepop}}{A_{C,postpop}}} = \sqrt{\frac{h_{C,prepop}}{h_{C,postpop}}} \tag{19}$$

According to HERTZ the elastic contact depth is half the total elastic penetration, i.e.

$$h_{C,prepop} = 0.5\delta_{prepop} \qquad h_{C,postpop} = h_t - 0.5\delta_{postpop} \tag{20}$$

$$\delta_{postpop} = \frac{\delta_{prepop}}{\sqrt{\frac{h_{C,postpop}}{h_{C,prepop}}}} = \frac{\delta_{prepop}}{\sqrt{\frac{h_t - 0.5\delta_{postpop}}{0.5\delta_{prepop}}}} \tag{21}$$

Equation (21) is suitable for iteration. For ease of demonstration let us consider the situation of $\delta_{postpop} = h_{pop} = a$. We thus have a total depth $h_t = 2a$ and $h_{C,prepop} = a/2$; starting the iteration with $\delta_{pospop,0} = a$ gives $h_{C,postpop,0} = 1.5a$. We obtain

$$\delta_{postpop,1} = a / \sqrt{1.5a / 0.5a} = a/\sqrt{3} = 0.58a$$

$$\delta_{postpop,\ 2} = a / \sqrt{(2a - 0.29\, a) / 0.5\, a} = 0.541\, a$$

$$\delta_{postpop,\ 3} = a / \sqrt{(2a - 0.27\ a) / 0.5\ a} = 0.538\ a$$

For the situation $h_{pop} = \delta_{prepop}$ a ratio $\delta_{postpop} / \delta_{prepop} = 0.54 \pm 0.005$ was found after 3 steps of iteration.

An interesting finding of the presented analysis is that the depth h_r of the remaining impression can be considerably larger than the depth excursion during the pop-in

event. For the given example one obtains $h_r = 2a - \delta_{postpop} = 1.46a = 1.46h_{pop}$. In table 1 numerical values for the ratios $(\delta_{prepop}/\delta_{postpop})$ and (h_r/h_{pop}) and for the plastic energy W_{pop} are displayed as a function of the relative depth excursion $\alpha = h_{pop}/\delta_{prepop}$. It turns out that for tiny pop events, i.e. small values of α, the final depth is three times as large as the depth excursion, and the plastic energy approaches a value of $W_{pop} = 1.8\ F_{pop}\ h_{pop}$. This can be shown as follows:

$$\frac{\delta_{postpop}}{\delta_{prepop}} = \sqrt{\frac{A_{C,prepop}}{A_{C,postpop}}} = \sqrt{\frac{h_{C,prepop}}{h_{C,postpop}}} = \sqrt{\frac{\delta_{prepop}/2}{\delta_{prepop} + h_{pop} - (\delta_{postpop}/2)}} \tag{22}$$

$$\frac{\delta_{postpop}}{\delta_{prepop}} = \sqrt{\frac{1}{2 + 2(h_{pop}/\delta_{prepop}) - (\delta_{postpop}/\delta_{prepop})}} \tag{23}$$

We now introduce $\delta_{postpop}/\delta_{prepop} = 1 - 2\alpha$ and obtain with $h_{pop}/\delta_{prepop} = \alpha$

$$\frac{\delta_{postpop}}{\delta_{prepop}} = \sqrt{\frac{1}{1+4\alpha}} \approx \sqrt{1-4\alpha} \approx 1-2\alpha \tag{24}$$

i.e. we obtain a result which is consistent to the introduced prediction. Furthermore one gets

$$h_r = \delta_{prepop} + h_{pop} - \delta_{postpop} = h_{pop} + 2\alpha\ \delta_{prepop} \tag{25}$$

$$h_r/h_{pop} = 1 + 2\alpha\ (\delta_{prepop}/h_{pop}) = 1 + 2\alpha\ (1/\alpha) = 3 \tag{26}$$

$$\delta_{postpop} - \delta_{prepop} = 2\alpha\ \delta_{prepop} = 2h_{pop} \tag{27}$$

$$W_{pop} = F_{pop}\ h_{pop} + 0.4\ F_{pop}\ (\delta_{postpop} - \delta_{prepop}) = 1.8\ F_{pop}\ h_{pop} \tag{28}$$

INSERT TABLE 1 ABOUT HERE

The most interesting outcome of table 1 is that for small pop-in events the remaining depth oh the impression grove is three times as large as the depth excursion, and the plastic work is almost double the value of $F_{pop}\ h_{pop}$. This theoretical finding was confirmed by experiments. Figure 5 displays the load-depth curve $F(h)$ for a Berkovich nanoindent into single-crystalline GaAs(100). The maximum load was 100µN, and this was by chance only a bit larger than the pop-in force of approximately 90µN. The depth excursion amounts to h_{pop} = 2nm, whereas the remaining depth is 6nm, i.e. three times as large. The average spacing between loading and unloading curve is d = 0.5(2nm + 6nm) = 4nm, i.e. twice as large as h_{pop}. The content of the loading-unloading loop amounts to $A_{loop} = W_{pop} \approx F_{pop}\ d \approx 2\ F_{pop}\ h_{pop}$ in good agreement to the theoretical value of $W_{pop} = 1.8\ F_{pop}\ h_{pop}$.

INSERT FIGURE 5 ABOUT HERE

3. The concept of differential hardness

The traditional nanohardness $H = F/A_C$ is the mean pressure inside the contact area of the indenter. If considering a multi-indentation test one can also divide the load increment ΔF from cycle to cycle by the corresponding increase of the contact area ΔA_C. This quantity is now introduced as "differential" hardness H_d:

$$H_d = \Delta F/\Delta A_C \tag{29}$$

The multi-indent delivers discrete values of H_d. In figure 6A values of H and H_d derived from multi-indentation testing of Cu (100) are depicted. The differential hardness was found to be smaller than the traditional hardness. As will be shown below this difference is related to the indentation size effect of Cu, i.e. the general decrease of hardness with increasing penetration depth in the nanorange. When considering materials of constant hardness, the values of H and H_d are equivalent.

INSERT FIGURE 6 ABOUT HERE

The differential hardness can also be derived from a single indent:

$$H_d = dF/dA_C = (dF/dh)/(dA_C/dh) \quad (30)$$

To calculate H_d we need the differential quotient dF/dh which is simply the slope of the $F(h)$-curve. Additionally, dA_C/dh is required which is not directly accessible from the experiment. However, we know A_C as a function of contact depth h_C. Thus we can write

$$dA_C/dh = (dA_C/dh_C)*(dh_C/dh) \quad (31)$$

(dA_C/dh_C) is accessible from the indenter shape calibration. Furthermore, we can assume that (dh_C/dh) is a function that exhibits small variations with depth h only. Thus we can write

$$dh_C/dh \approx h_C/h \quad (32)$$

where h_C and h are the values of contact depth and total depth taken from the final unloading procedure. This results in

$$H_d = (dF/dh)/[(dA_C/dh_C)*(dh_C/dh)] \approx (h/h_C)*(dF/dh)/(dA_C/dh_C) \quad (33)$$

4. Relation between traditional hardness H and differential hardness H_d

We start with the definition of classical hardness $H = F/A_C$ and perform some simple transformations:

$$HA_C = F \quad (34)$$

$$HA_C = \int dF = \int \frac{dF}{dA_C} * \frac{dA_C}{dh} * dh = \int H_d * \frac{dA_C}{dh} * dh \quad (35)$$

After the operations (d/dh) and division by (dA_C/dh) one obtains

$$H_d = H + \frac{dH}{dh} * \frac{A_C}{(dA_C/dh_C)(dh_C/dh)} \quad (36)$$

For an ideal pointed indenter (pyramid / cone) the area function is $A_C = C_A h_C^2$, resulting in $dA_C/dh_C = 2C_A h_C$. This in combination with $dh_C/dh \approx h_C/h$ delivers

$$H_d = H + \frac{1}{2}\frac{dH}{dh} * h \quad (37)$$

We see that for missing indentation size effect ($dH/dh = 0$) the relation $H_d = H$ is obtained. The normal indentation size effect ($dH/dh < 0$) results in a differential

hardness which is smaller than H. Such a situation can be found with tiny indentations into single-crystalline metals where the hardness can be described following the model of geometrical necessary dislocations [16, 17], as in the case of copper, e.g. . The model of geometrical necessary dislocations predicts a depth dependence of H according to

$$H = H_0 \sqrt{\frac{h^*}{h}} \tag{38}$$

with H_0 and h^* being scaling parameters that depend on the defect structure of the metal. This delivers

$$H_d = H + \frac{1}{2}\frac{dH}{dh}h = (3/4)\,H \tag{39}$$

A closer look to figure 6B reveals that H_d/H indeed scatters around 0.75 with a slight tendency to increase with deeper penetration which is further discussed in the following section.

5. Application of differential hardness and conclusions

The differential hardness as a differential entity is of course more inclined to scatter and it is more sensitive to measurement errors than traditional hardness or integral techniques as the derivation of an energetic hardness from the plastic work during indentation, e.g. Since H_d and H have the same value for homogeneous materials and self-similar indents the application of the differential hardness concept to such situations does indeed not provide new information. The situation is completely different with inhomogeneous samples, as layer systems, e. g. It should be noticed here that even a small pyramid indent into a single crystal will not obey the criteria of self-similarity though the indentation body is self similar. The deformation can be roughly separated into two stages:

Stage I: Small penetrations where the indent size is not much larger than the mean distance between hardness determining crystal defects. Here the hardness is governed by dislocations and other defects created by the indenter itself. The density of these defects depends on indent size, consequently the situation is not self-similar, and the hardness varies.

Stage II: Large penetrations, where the hardness is determined by intrinsically existing lattice defects. Provided the defect distribution is homogeneous the indent is self-similar, and the hardness is constant. Then $dH/dh = 0$, and $H_d/H = 1$ is found.

The slow increase of H_d/H in figure 6B indicates the transition from stage I to stage II, and from the trend may be concluded that stage II will dominate after about 2µm of penetration.

In case of "really" inhomogeneous specimens as layered materials one wants to know the single layer properties, but even the depth dependent hardness is no direct measure of the material property at the corresponding depth owing to the averaging over a larger deformed volume. To extract the real material property in a certain depth a deconvolution must be made. To do this one has to know to what extent material properties at a depth $h + \Delta h$ contribute to the measured data at depth h. It is reasonable to assume, that these contributions to H and H_d are different. Hence H_d is an additional source of information to make the deconvolution procedure more straightforward.

Another field of application are processes that occur during the indentation test itself and modify the sample hardness. As an example the photoplastic effect (PPE) shall be

considered here. Some materials – II-VI-semiconductors in particular – change their hardness reversibly when illuminated by light the photon energy of which is sufficient to initiate the internal photo-electric effect. This finding is explained by electrical charging of dislocations [18]; indentation studies of the PPE in ZnSe have been reported in [19]. Figure 7 displays two load-depth-curves $F(h)$ of nanoindentations into the II-VI-semiconductor ZnSe. The sudden change of the slope of curve 1 was induced by turning a laser on which resulted in a positive photoplastic effect (reverse material hardening). Curve 2 belongs to an indentation completely performed in darkness. The difference of the final penetrations between curves 1 and 2 is about 30nm or 5% of the total depth, resulting in about 10% hardness change, only (for pyramid indenters the relative hardness change is about twice the relative depth variation). This apparently small effect originates from the fact that the illumination was turned on close to the end of the indentation process when most of the deformation was already done. On the other hand the slope changes from $(dF/dh)_{dark} = 47\mu N/nm$ to $(dF/dh)_{light} = 83\mu N/nm$. This means, that the differential hardness – representing the instantaneous deformation resistance – has almost doubled in contrast to the "traditional" hardness, which increased by 10%. When modulating the light intensity the penetration curve oscillates, and the differential hardness proves a suitable tool to track the corresponding hardness evolution. Summarizing we can say, that the differential hardness may be particularly advantageous when time dependent processes that affect the hardness occur during the indentation process itself.

INSERT FIGURE 7 ABOUT HERE

Acknowledgments

The experimental results used in this paper were obtained during stays of the author at Technische Universität Dresden, Technische Fachhochschule Wildau (Laboratory of Surface Physics, Prof. Asta Richter) and Universität des Saarlandes, Saarbrücken. The author would like to express his gratitude to the staff of these institutions for very fruitful cooperation.

References

[1] D. Tabor, *The hardness of metals* (Clarendon Press, Oxford, 1951).

[2] B.W. Mott, *Micro-indentation hardness testing* (Butterworths, London, 1956).

[3] J.L. Hay, G.M. Pharr, in *ASM Metals Handbook* (ASM International, Materials Park, Ohio, 2000).

[4] B. Wolf and P. Paufler, phys. stat. sol. (a) **172** 341 (1999).

[5] B. Bhushan, in *Springer Handbook of Nanotechnology*, edited by B. Bhushan (Springer, Berlin, New York, 2004) Chapter 22, pp. 685 - 714.

[6] Nano Instruments Website (2006 MTS Systems Corporation) available online at: http://www.mtsnano.com/products/csm/

[7] W.C. Oliver and G.M. Pharr, J. Mater. Res. **7** 1564 (1992).

[8] W.C. Oliver and G.M. Pharr, J. Mater. Res. **19** 3 (2004).

[9] B. Wolf, A. Richter and M. Günther, Z. Metallkd. **94** 807 (2003).

[10] D.F. Bahr, D.E. Wilson and D.A. Crowson, J. Mater. Res. **14** 2269 (1999).

[11] E.B. Tadmor, R. Miller, R. Phillips and M. Ortiz, J. Mater. Res. **14** 2233 (1999).

[12] B. Wolf, Cryst. Res. Technol. **35** 377 (2000).

[13] A. Zeckzer, Anisotropie der Versetzungsnukleation in GaAs bei Nanoindentierung, PhD thesis, Martin-Luther-Universität Halle-Wittenberg (2002).

[14] H. Hertz, J. reine und angewandte Mathematik **92** 156 (1882).

[15] K.L. Johnson, *Contact mechanics* (Cambridge University Press, Cambridge, 1985).

[16] M.F. Ashby, Phil. Mag. **21** 399 (1970).

[17] S. Sun, B.L. Adams and W.E. King, Phil. Mag. **A80** 9 (2000).

[18] Yu.A.Osiyan, V.F. Petrenko, A.V. Zaretskij and R.W. Whitworth, Adv. Phys. **35** 115 (1986).

[19] B. Wolf, A. Belger, D.C. Meyer and P. Paufler, phys. stat. sol. (a) **187** 415 (2001) and Phil. Mag. A **82** 1865 (2002).

Figure Captions / Table Legends

Figure 1
Principal sketch of the unloading-reloading-behaviour for materials with a small stress exponent n of creep (left graph) and a large stress exponent (right graph). For large values of n significant creep occurs in the vicinity of the maximum load only; for small n creep persists during entire unloading and reloading.

Fig. 2.
Load – depth-curves $F(h)$ of cube-corner indentations into CdS(0001)
Curve 1: Single indent
Curve 2: Multi-indent (18 cycles)
For better comparison curve 1 was vertically shifted by 0.3mN.

Fig. 3.
Hardness values derived from iterative analysis of a single indent (graph 1 in figure 2) compared to corresponding values inferred from a multicycling indentation (graph 2 in figure 2). The iteration procedure converges rapidly (iteration 2 is almost identical to iteration 1) and the obtained results are in good agreement to the multi-indentation data.

Figure 4
Schematical representation of the hysteresis loop of a strain burst event (left part). The areas beneath loading and unloading curves (regions I and II) are not equivalent, since the unloading is stiffer, resulting in $\delta_{prepop} < \delta_{postpop}$. Consequently, $W_{pop} > F_{pop}\, h_{pop}$ (right part).

Fig. 5
Cube corner nanoindentation into GaAs (100). By chance the pop-in event occurs close to the termination of the loading segment which permits an experimental test of the predictions of table 1.

Figure 6
A) Traditional nanohardness data $H = F/A_C$ compared to corresponding values of the differential hardness $H_d = \Delta F/\Delta A_C$ as taken from multi-indentation testing of Cu (100).
B) Ratio H_d/H for the measurement of figure 6A exhibiting a typical value of $H_d/H \approx 0.75$ with the tendency of a slight increase from about 0.73 to 0.85 with increasing depth as indicated by the trend line.

Figure 7.
Response of the load-depth-curve of a Berkovich nanoindention into ZnSe (111) to sudden illumination by laser light (λ = 543nm, intensity I = 120mW/cm^2). Curve 1: starting the indent in darkness the laser was turned on at a total depth h = 600nm. Curve 2: indentation in permanent darkness.

Table legends

Table 1
Characteristic quantities of a loading-unloading loop involving a depth excursion. The data were calculated as a function of the relative depth excursion amplitude $\alpha = h_{pop}/\delta_{prepop}$

Figures

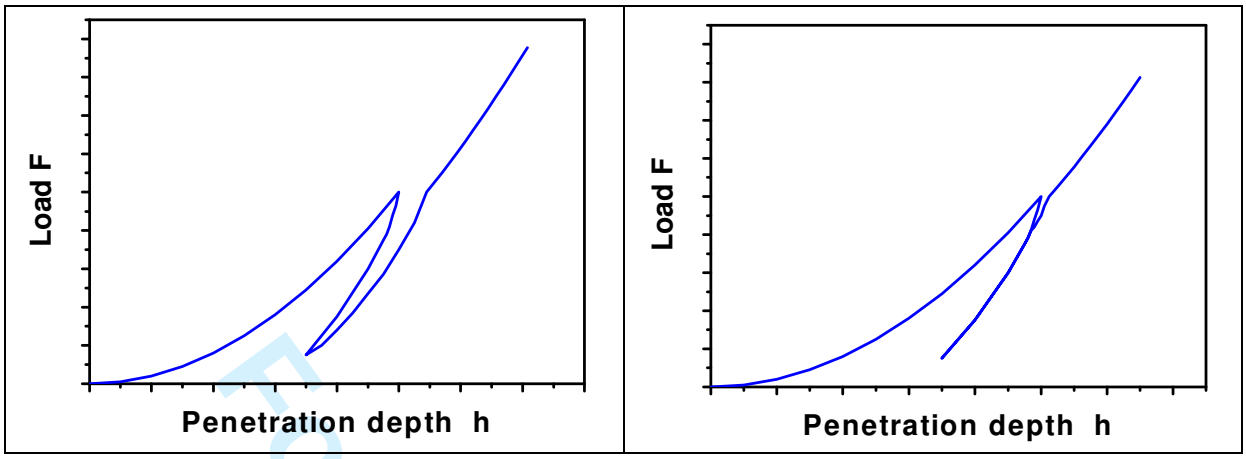

Figure 1
Principal sketch of the unloading-reloading-behaviour for materials with a small stress exponent *n* of creep (left graph) and a large stress exponent (right graph). For large values of *n* significant creep occurs in the vicinity of the maximum load only; for small *n* creep persists during entire unloading and reloading.

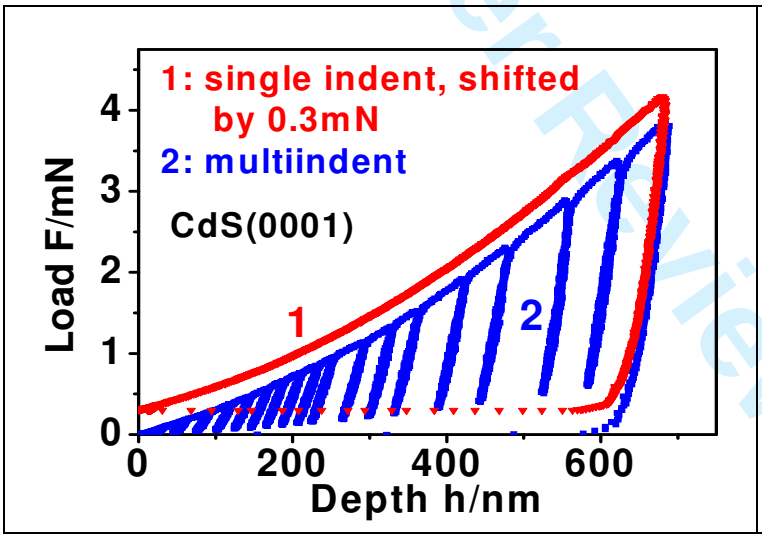

Fig. 2.
Load – depth-curves $F(h)$ of cube-corner indentations into CdS(0001)
Curve 1: Single indent
Curve 2: Multi-indent (18 cycles)
For better comparison curve 1 has been vertically shifted by 0.3mN.

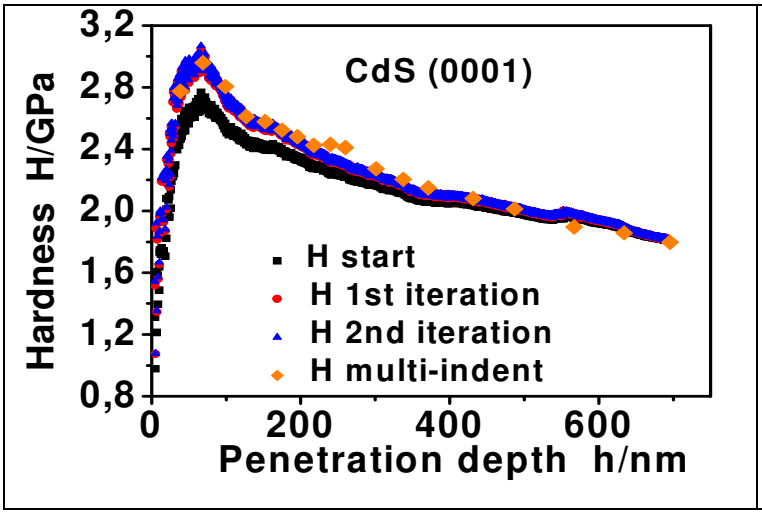

Fig. 3.
Hardness values derived from iterative analysis of a single indent (graph 1 in figure 2) compared to corresponding values inferred from a multicycling indentation (graph 2 in figure 2). The iteration procedure converges rapidly (iteration 2 is almost identical to iteration 1) and the obtained results are in good agreement to the multi-indentation data.

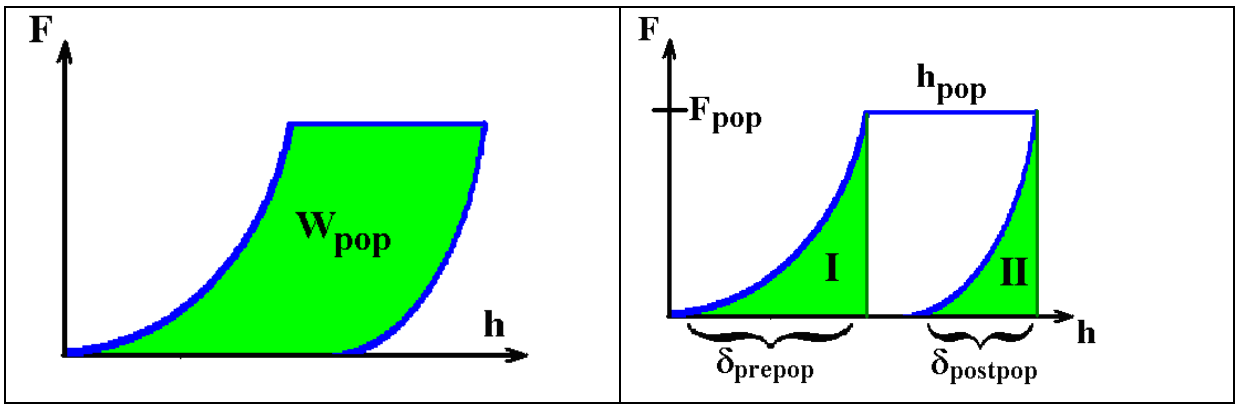

Figure 4
Schematical representation of the hysteresis loop of a strain burst event (left part). The areas beneath loading and unloading curve (regions I and II) are not equivalent, since the unloading is stiffer, resulting in $\delta_{prepop} < \delta_{postpop}$. Consequently, $W_{pop} > F_{pop}\, h_{pop}$ (right part).

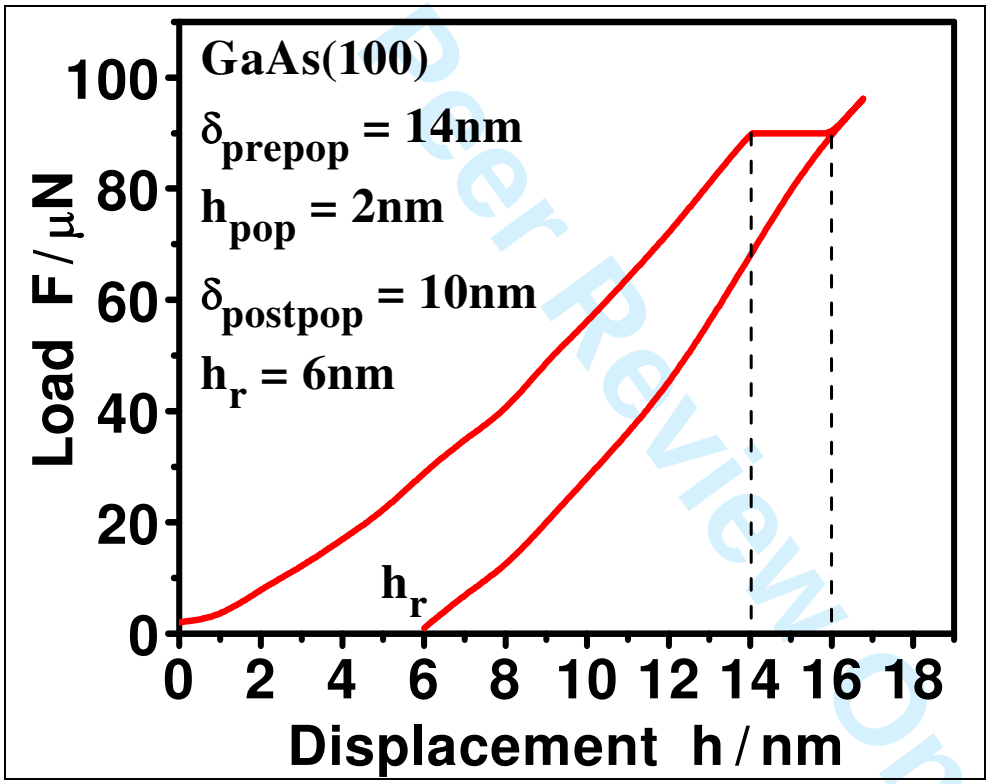

Fig. 5
Cube corner nanoindentation into GaAs (100). By chance the pop-in event occurs close to the termination of the loading segment which permits an experimental test of the predictions of Table 1.

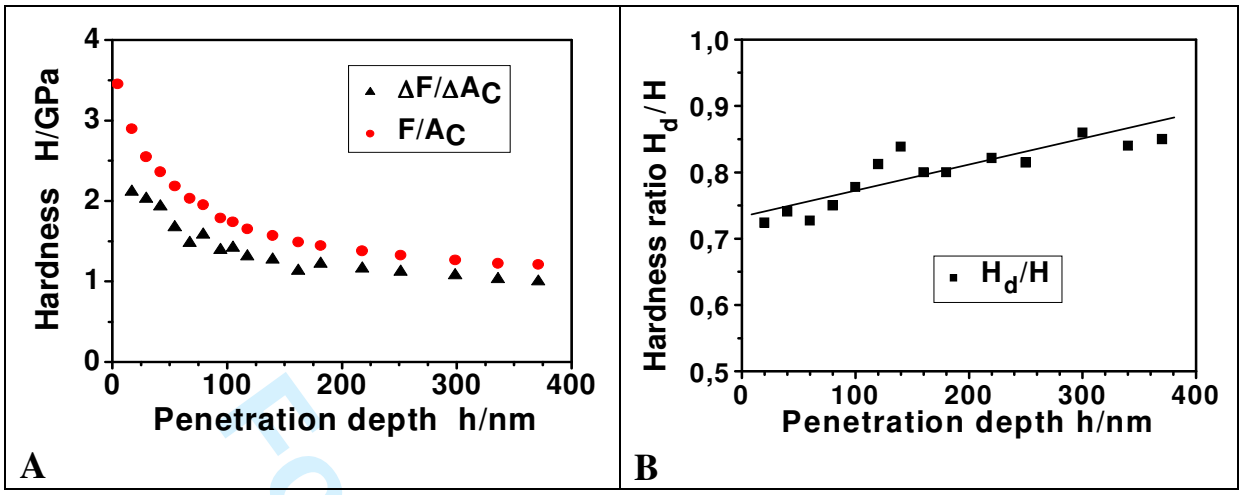

Figure 6
A) Traditional nanohardness data $H = F/A_C$ compared to corresponding values of the differential hardness $H_d = \Delta F/\Delta A_C$ as taken from multi-indentation testing of Cu (100).
B) Ratio H_d/H for the measurement of figure 6A exhibiting a typical value of $H_d/H \approx 0.75$ with the tendency of a slight increase from about 0.73 to 0.85 with increasing depth as indicated by the trend line.

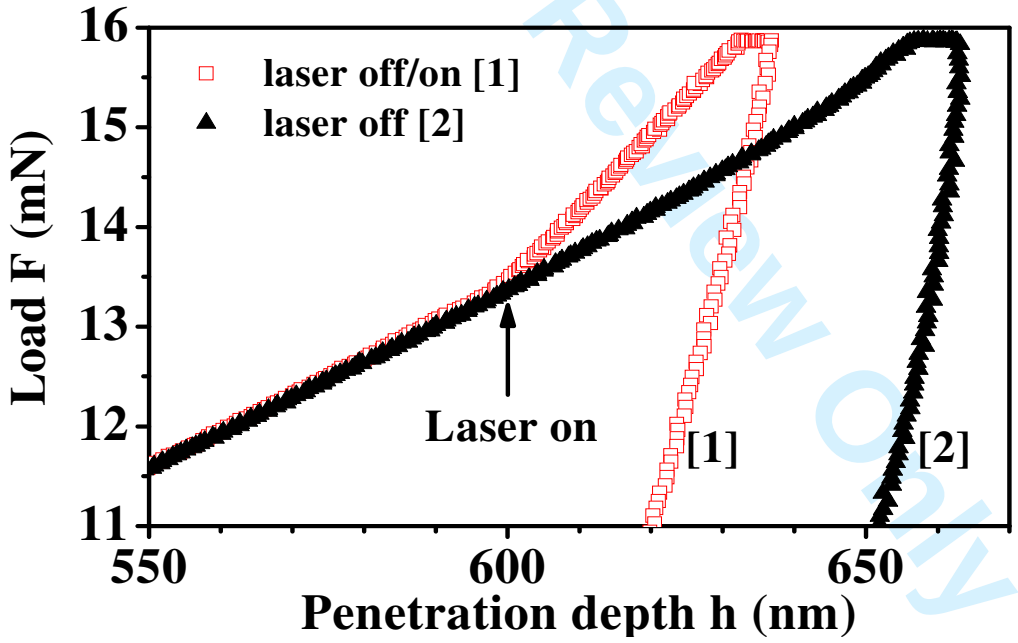

Figure 7.
Response of the load-depth-curve of a Berkovich nanoindention into ZnSe (111) to sudden illumination by laser light (λ = 543nm, intensity I = 120mW/cm^2). Curve 1: starting the indent in darkness the laser was turned on at a total depth h = 600nm. Curve 2: indentation in permanent darkness.

Classical and differential hardness – aspects of quantifying the deformation response in indentation experiments

BODO WOLF

Fachhochschule Lausitz , Fachbereich IEM, Großenhainer Straße 57, D-01968 Senftenberg, Germany

Tables

relative depth excursion $\alpha = h_{pop}/\delta_{prepop}$	$\frac{\delta_{postpop}}{\delta_{prepop}}$	$\frac{h_r}{h_{pop}}$	Plastic energy W_{pop}
2	0.423	1.288	1.12 F_{pop} h_{pop}
1	0.537	1.463	1.19 F_{pop} h_{pop}
0.5	0.653	1.694	1.27 F_{pop} h_{pop}
0,2	0.788	2.06	1.42 F_{pop} h_{pop}
0.1	0.867	2.33	1.53 F_{pop} h_{pop}
0.01	0.981	2.90	1.77 F_{pop} h_{pop}
0.001	0.9980	3.00	1.80 F_{pop} h_{pop}
$\alpha << 1$	$1 - 2\alpha$	3.00	1.80 F_{pop} h_{pop}

Table 1